Journal of Materials Science: Materials in Electronics (2018) 29:21194–21204
https://doi.org/10.1007/s10854-018-0269-5

Enhanced electrochemical performance of $MnCo_2O_4$ nanorods synthesized via microwave hydrothermal method for supercapacitor applications

S. Jayasubramaniyan[1,2] · S. Balasundari[2,3] · P. A. Rayjada[4] · R. Arockia Kumar[5] · N. Satyanarayana[6] · P. Muralidharan[2]

Received: 15 July 2018 / Accepted: 21 October 2018 / Published online: 25 October 2018

Abstract
$MnCo_2O_4$ nanorods were facilely prepared via microwave hydrothermal method. X-ray diffraction pattern showed pure crystalline spinel phase $MnCo_2O_4$ formation for the calcined powder at 400 °C. Fourier transform infrared spectroscopy (FTIR) spectrum of the $MnCo_2O_4$ powders showed the strong vibrational modes of Mn–O and Co–O bonds. Raman spectrum showed the structural bonding features and crystalline nature of $MnCo_2O_4$. Scanning electron microscopy images exposed a morphology that shows the aggregation of several nanorods to form bundles of nanorods ~ 300–400 nm in diameter and few microns in length. Energy-dispersive spectrometry analysis confirmed the presence of Mn, Co, O elements for the powder calcined at 400 °C. The electrochemical characterization of the $MnCo_2O_4$ nanorods with 1 M KOH as the electrolyte exhibited an excellent capacitance of 2394.4 F g^{-1} at a scan rate of 5 mV s^{-1} and revealed a highest specific capacitance of 1617.5 F g^{-1} from the galvanostatic charge/discharge analysis at a current density of 1 A g^{-1}. The cycling stability at different current densities revealed the high rate performances and good reversible capacity retention of the calcined $MnCo_2O_4$ nanorods. The cycling life study of $MnCo_2O_4$ nanorods demonstrated an excellent cycling stability with 88% of the initial specific capacitance retention at 10 A g^{-1} after 1000 cycles.

1 Introduction

The rapid development in energy utilization by the miniaturized portable electronic devices to a hybrid electric vehicle requires extensive improvement in the energy technologies. The most efficient energy storage device is the electrochemical capacitor or supercapacitors because of their high speed of the charge–discharge process, long time durability, cycle stability, enhanced energy and power density compared with batteries [1–4]. Generally, the supercapacitor can be classified as an electric double layer capacitor (EDLC) and redox- or pseudocapacitor based on the energy storage mechanism [5]. The EDLC works with respect to accumulation of electrical charge by electrostatic separation at electrode/electrolyte interfaces. On the other hand, the pseudocapacitors works based on the fast redox reaction on the surface or around the surface region of the electrodes, where electrosorption/electrodesorption occurs with charge transfer but without any bulk phase transformation upon charging/discharging. As a result, pseudocapacitors deliver a high specific capacitance than the EDLCs [6–8]. The binary metal oxides, particularly designated as MCo_2O_4 (M = Mn, Ni, Cu etc.) are one of the promising electrode materials for pseudocapacitor. These oxides are efficient alternatives to the carbon-based materials due to their advantages such as excellent performances, multiple oxidation states, fast redox reaction, low cost, and eco-friendly compared to other electrode materials. In recent years, $MnCo_2O_4$ has found

✉ P. Muralidharan
dharan9@gmail.com

1 Research and Development Centre, Bharathiar University, Coimbatore 641046, India

2 Centre for Advanced Materials Engineering Research and Application, (CAMERA), Department of Chemistry, Rajiv Gandhi College of Engineering and Technology, Kirumampakkam, Puducherry 607403, India

3 Department of Chemistry, Arignar Anna Government Arts College, Villupuram 605 602, India

4 Fusion Fuel Cycle Division, Institute for Plasma Research, Gandhinagar 382010, India

5 Department of Metallurgical and Materials Engineering, National Institute of Technology (NIT), Warangal 506004, India

6 Department of Physics, Pondicherry University, Kalapet, Puducherry 605014, India

to be a substitute electrode material for supercapacitor due to their high theoretical capacitance (~ 3619 F g^{-1}) and it demonstrates the superior capacitive performance and high electrochemical performance compared to other binary metal oxides [9–15]. However, the experimentally achieved capacity of pure $MnCo_2O_4$ is lower than the theoretical value, which is due to their low electrical conductivity, high electron transfer resistance and poor electrolyte utilization efficiency active materials [16–18].

The morphology of the electrode material finds a significant role in the reduction of the electron transfer resistance and improving the efficiency of active material utilization by the electrolyte ions and this determines the efficiency of the device because the ion diffusion and conductivity are directly depended on the morphology of the electrode material [19]. From the literature survey, it has been identified that the various morphologies of $MnCo_2O_4$ synthesized and tested for its feasibility as a supercapacitor electrode. Li et al., has reported that the prepared one-dimensional $MnCo_2O_4$ nanowire directly on the nickel foam showed a capacitance of 349.8 F g^{-1} at 1 A g^{-1} [20]. Kong et al., has reported that the prepared $MnCo_2O_4$ nanoparticles showed a specific capacitance 405 F g^{-1} at 5 mA cm^{-2} [21]. Xu et al. synthesized porous $MnCo_2O_4$ nanowires, which exhibited a significant specific capacitance of 1342 F g^{-1} at 1 A g^{-1} [16]. Venkatachalam et al., has reported the synthesized $MnCo_2O_4$ nanorods exhibited 718.75 F g^{-1} at a current density of 0.5 A g^{-1} [22]. Krishnan et al., has reported that the prepared $MnCo_2O_4$ flakes and it exhibited 600 F g^{-1} at a current density of 0.5 A g^{-1} [23]. Hui et al., has reported that successfully prepared chestnut-like $MnCo_2O_4$ nanoneedles on nickel and it shows excellent capacitance of 1535 F g^{-1} at a current density of 1 A g^{-1} [18]. Thorat et al., has reported that the synthesized $MnCo_2O_4$ microspheres exhibited 950 F g^{-1} at a current density of 2 A g^{-1} [24]. Thus the literature reports reveal that by controlling the particle size of the electrode material and achieving good morphology with the high surface area is an alternative technique to enhance the pseudocapacitive performance of the binary metal oxide electrodes. In this point of view, various synthetic approaches developed to control the size as well as the morphology of the electrode material, and thereby electrochemical capacitance, ion transport, electrical conductivity, the cyclic reversible performance of the metal oxides can be improved [25, 26]. Recently, microwave hydrothermal (MH) assisted synthesis method is utilized to prepare oxide, hydroxide, and sulfide nanoparticles with various morphologies. The advantages of the MH method are simple, clean, fast reaction time, energy and time-saving process and the morphology of materials are in control, without thermal gradient effects problems [19, 27–30].

The present work focuses on the facile synthesis of the $MnCo_2O_4$ nanostructure material via the MH method. The calcined powder samples are characterized by X-ray diffraction (XRD), Fourier-transform infrared spectroscopy (FTIR), Raman spectroscopy, Field emission scanning electron microscopy (FE-SEM), and Electrochemical performances and cycle stability at various current densities and longtime cyclic stability with high current density are studied and compared with the reported literature results.

2 Experimental

2.1 Materials and methods

Analar grade precursor chemicals manganese nitrate hexahydrate $Mn(NO_3)_2{\cdot}6H_2O$ [Merck, 99.9%], cobalt nitrate hexahydrate $Co(NO_3)_2{\cdot}6H_2O$ [Merck, 99.9%], absolute ethanol (China) and de-ionized (DI) water were used as purchased without further purification. Nickel foam (1.6 mm thickness) was purchased from MTI Corporation (China). The Microwave-hydrothermal synthesis has been carried out in a Microwave reaction system SOLV Multiwave PRO, Anton Paar, Germany.

2.2 Preparation of $MnCo_2O_4$

In a typical synthesis, 0.01 mol of manganese nitrate hexahydrate $Mn(NO_3)$ $6H_2O$ and 0.02 mol of cobalt nitrate hexahydrate $Co(NO_3)_2{\cdot}6H_2O$ were dissolved in 250 ml of deionized (DI) water. The solution was stirred for 1 h at room temperature to attain a homogeneous transparent solution. Then the homogeneous clear solution was transferred into the quartz vessels and placed on a rotatable stage for uniform heat treatment at 180 °C for 15 min in a microwave reaction system SOLV, Multiwave PRO Anton-Paar. After the reaction completion, the reaction quartz vessels were cooled to room temperature. Thus obtained brown colour precipitate was carefully transferred, filtered and washed with distilled water and absolute ethanol. The obtained brown colour precipitate was dried in an oven at 60–70 °C for 12 h and followed by calcination at 400 °C for 3 h to form $MnCo_2O_4$ nanostructure material.

2.3 Materials characterization

The synthesized samples were characterized with a powder X-ray diffractometer (X'pert PRO MPD, PANalytical) employing Cu Kα radiation (λ = 0.15406 nm), angles ranging from 10° to 80° with step size 0.02. The structural bonding nature of the powders was recorded using Thermo Nicolet FTIR-6700 spectrometers from 4000 to 400 cm^{-1} for 30 scans for the thin transparent pellets. The transparent pellet was made using 400 °C calcined powders for 3 h and grounded well with pure KBr crystalline powder taken

in 1:20 ratio. Raman spectra were recorded in the range 100–2000 nm using RENISHAW inVia confocal Raman microscope, UK, with 785 nm line of an argon ion laser, keeping their maximum output power at 100 mW The morphology and microstructure of the calcined powder at 400 °C for 3 h were characterized using a field emission scanning electron microscope (FE-SEM, JSM-6700F, JEOL Ltd).

2.4 Electrochemical characterization

The working electrode was prepared by mixing the active material $MnCo_2O_4$ powder, carbon black as a conducting agent and polyvinylidene difluoride as a binder with the mass ratio 80:10:10 to obtain a homogeneous slurry with *N*-methyl pyrrolidone. Prior to coating the electrode material the nickel foam was cleaned with 6 M HCl aqueous solution in an ultrasound bath for 25 min and rinsed with DI water and absolute ethanol several times in order to eliminate the NiO layer on the surface. Then the homogeneous slurry was placed and pressed onto Ni foam and dried under vacuum at 80 °C for 24 h. A three-electrode cell consists of the working electrode, platinum as the counter electrode and saturated calomel electrode as a reference electrode were used and 1 M potassium hydroxide (1 M KOH) was used as the electrolyte. The electrochemical behavior of the $MnCo_2O_4$ electrodes was characterized by cyclic voltammetry (CV), galvanostatic charge/discharge (GCD) tests, electrochemical impedance spectroscopy (EIS) and cyclic stability using PARSTAT MC Multi-Channel Electrochemical workstation (Ametek, USA). EIS measurement was carried out in the frequency range of 10^4–1 Hz with a perturbation amplitude of 5 mV at open circuit potential.

3 Results and discussion

3.1 Characterization of $MnCo_2O_4$

XRD pattern of the $MnCo_2O_4$ powder prepared via the MH method and calcined at 400 °C for 3 h is shown in Fig. 1. From Fig. 1, it is observed that the XRD pattern shows diffraction peaks at the 2 theta values of 18.53, 30.52, 36.02, 37.61, 43.75, 54.32, 57.90 and 63.63°, which are assigned to (111), (220), (311), (222), (400), (422), (511) and (440) crystal planes. These crystal planes confirm the spinel $MnCo_2O_4$ compound formed at 400 °C. The XRD patterns of the $MnCo_2O_4$ are excellently matching with the standard JCPDS card no. 023-1237 [22]. There are no extra peaks other than those attributed to $MnCo_2O_4$, which illustrates the phase purity of the prepared $MnCo_2O_4$ compound. The broadening of diffraction peaks was observed in the XRD pattern and it indicates the small crystal size. The JCPDS file reveals that manganese and cobalt ions

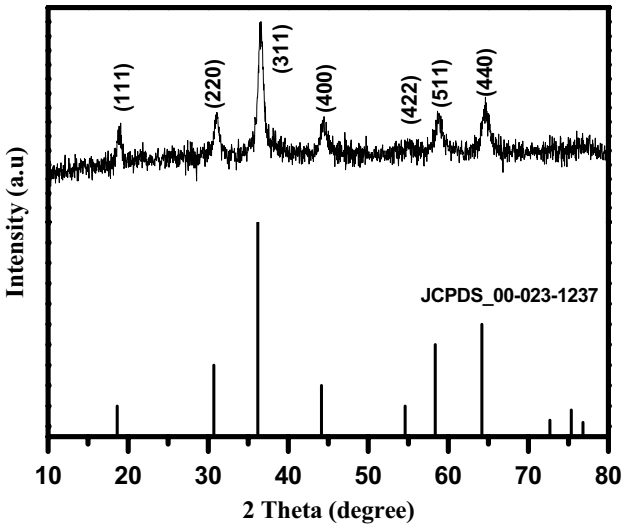

Fig. 1 XRD patterns of the $MnCo_2O_4$ powder calcined at 400 °C for 3 h

present in their mixed valence states in the $MnCo_2O_4$ spinel structure and both of them forms a cubic spinel structure with the +2 and +3 valence states. In the spinel, structured tetrahedral sites are occupied by the Mn^{2+} and Co^{2+} and the octahedral sites are occupied with the Mn^{3+} and Co^{3+} [31]. The crystallite size of the $MnCo_2O_4$ powders was calculated using the Scherrer's equation; $t = 0.9\lambda/\beta\cos\theta$, where t is the average crystallite size, λ is the wavelength of incident X-rays of Cu Kα radiation, β is the full width half maxima of the diffraction peak and θ is the Bragg diffraction angle [30]. The calculated crystallite si for the $MnCo_2O_4$ compound is about 21 nm.

FTIR spectrum of the $MnCo_2O_4$ nanopowder calcined at 400 °C for 3 h is shown in Fig. 2. From Fig. 2, it is observed that the strong transmittance bands at 651 and 559 cm^{-1} are attributed to the stretching vibrational modes of the spinel $MnCo_2O_4$ compounds [22]. These two bands are due to the interaction of tetrahedrally coordinated Mn^{2+}, Co^{2+} and octahedrally coordinated Mn^{3+}, Co^{2+} ions with the oxygen in the spinel $MnCo_2O_4$ structure. The peaks in the spectrum further confirm the presence of phase pure spinel $MnCo_2O_4$ and it also validates the pure phase results of XRD analysis.

Raman spectrum of the $MnCo_2O_4$ nanopowder calcined at 400 °C for 3 h is shown in Fig. 3. From Fig. 3, it observed that the spectrum shows five Raman bands in the region 100–1000 cm^{-1} positioned at 193, 479, 512, 609, and 679 cm^{-1} are related to the Raman-active modes Mn–O, Co–O of cubic spinel oxides $MnCo_2O_4$ [32]. The Raman modes confirm the formation of spinel $MnCo_2O_4$. Also, the absence of Mn–OH and Co–OH bands or other related bands in the spectrum confirms the formation of the spinel oxide $MnCo_2O_4$ [32, 33].

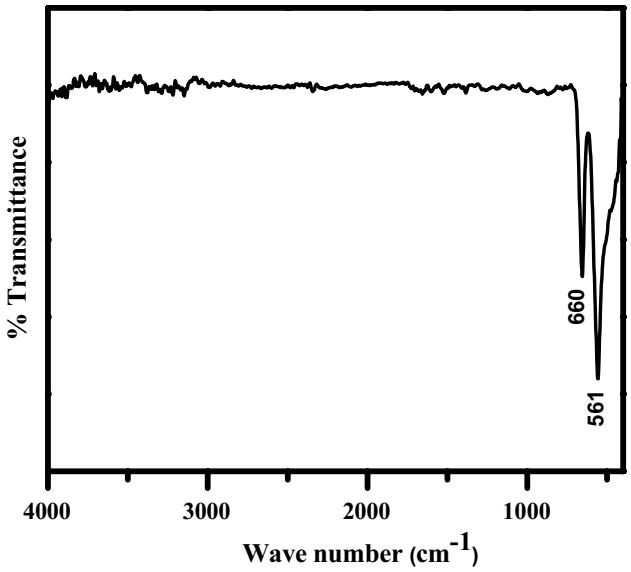

Fig. 2 FTIR spectrum of the $MnCo_2O_4$ powder calcined at 400 °C for 3 h

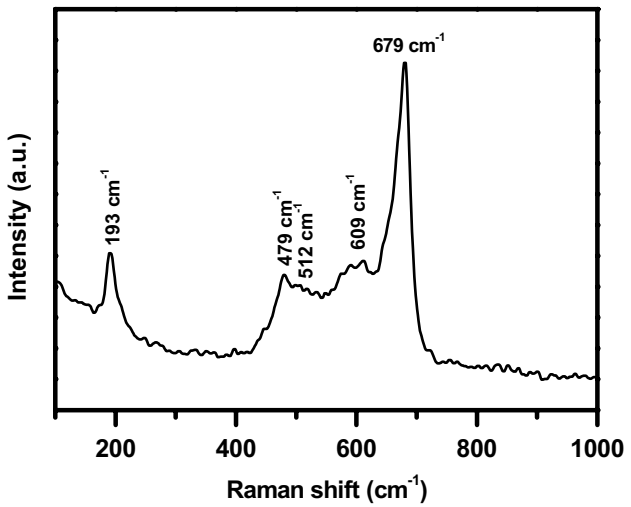

Fig. 3 Raman spectrum of the $MnCo_2O_4$ powder calcined at 400 °C for 3 h

The SEM micrograph images of the $MnCo_2O_4$ nanopowder calcined at 400 °C for 3 h is shown in Fig. 4. From Fig. 4, it is observed that the SEM micrographs scanned at different magnifications expose the presence the aggregation of several nanorods to form bundles of nanorods of ~300–400 nm in diameters and few microns in length. These aggregated bundles of nanorods like structure can facilitate the maximum access of electrolyte ion from bulk solution. In order to identify the elemental composition presence, the elemental analysis was performed using energy-dispersive spectrometry (EDS) and it is shown in Fig. 5. The EDS spectrum confirms the presence of Mn, Co and O. The percentage composition of Mn, Co and O of the nanorods surface clearly confirmed the atomic ratios of Mn, Co, and O present in 1:2:4 ratio.

3.2 Electrochemical analysis

The CV curves of the $MnCo_2O_4$ electrode at different scan rates from 5 to 100 mV s^{-1} using 1 M KOH as the electrolyte in the potential range of 0–0.6 V are shown in Fig. 6. In Fig. 6, the CV curves show the presence of redox peak which is due to the reversible transition between the oxidation states of cobalt (Co^{2+} and $Co^{3+)}$ and manganese ions (Mn^{2+} and Mn^{3+}). The anodic peak at around 0.35 V and the cathodic peak at around 0.1 V may correspond to the oxidation and the reduction process, respectively. The CV curve shows that the capacitance arises mainly due to reversible redox reactions of the electrode materials [22].

The reversible redox reaction mechanism may be described by the following equation

$$MnCo_2O_4 + H_2O + OH^- \rightarrow MnOOH + CoOOH + e^-$$

$$MnOOH + OH^- \rightarrow MnO_2 + H_2O + e^-$$

$$CoOOH + OH^- \leftrightarrow CoO_2 + H_2O + e^-$$

The CV curves do not contain separate cathodic and anodic peaks for cobalt and manganese ions and it reveals that the cobalt and manganese ions were identical in their electrochemical reactivity [34]. The shapes of the CV curves do not change at different scan rates, 5–100 mV s^{-1}, but the CV curves peak positions widely shift with increased scan rate. The oxidation peaks gradually move to higher potentials, whereas the reduction peaks shift to lower potentials in the opposite directions. As a result, it is identified that at higher scan rates the electronic and ionic movements are rapid and a fast redox reaction occurs at the interface of electroactive material/electrolyte [35, 36]. The capacitance arises from the material can be determined from the relationship between peak current with the square root of the scan rate. As a result, it confirms that either the capacitance arises from the surface redox reactions or from the bulk diffusion. The peak current versus the square root of the scan rate of the $MnCo_2O_4$ nanorods bundles is shown in Fig. 7. It shows a linear relationship of peak current with square root scan rate, which indicates the electrode reaction is diffusion-controlled. Moreover, it shows that the electrochemical process is controlled by the diffusion of OH^- ions [37]. The specific capacitances are calculated for the electrodes using the CV data and GCD data in Eqs. (1) and (2), respectively,

$$C_s = \frac{Q}{\Delta V m} \mathrm{F\ g^{-1}} \quad (1)$$

$$C_s = \frac{I \Delta t}{m \Delta V} \mathrm{F\ g^{-1}} \quad (2)$$

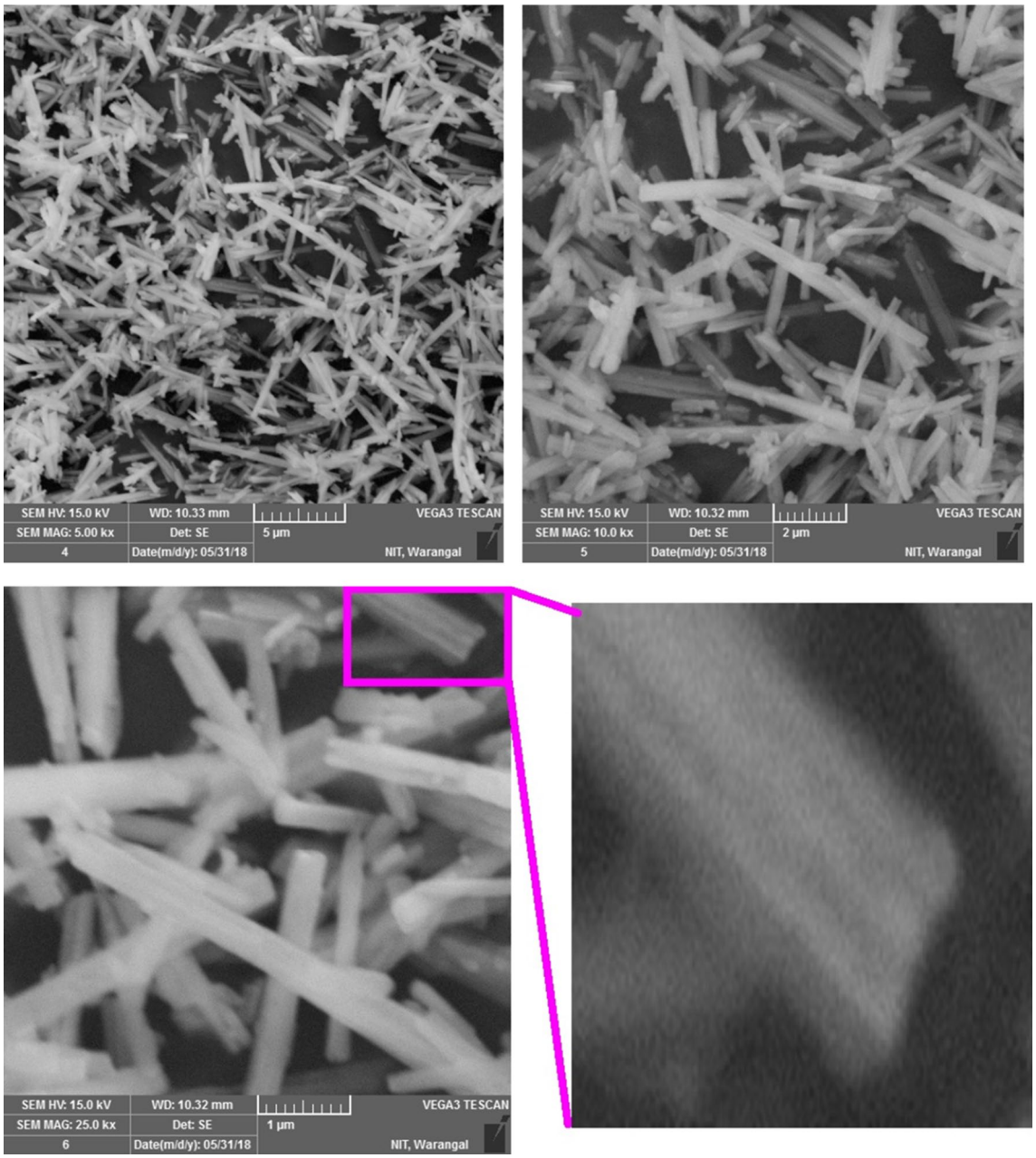

Fig. 4 SEM images scanned at different magnification and enlarged view of the $MnCo_2O_4$ powder calcined at 400 °C for 3 h

where Cs is the specific capacitance, Q is the average charge of the electrode (Coulomb), ΔV is the potential window (V), m is the loaded mass of the active material (g), I is the discharge current (A) and Δt is the discharge time (s) [38, 39]. The calculated Cs for the $MnCo_2O_4$ nanorods bundles are 2394, 1671, 1121, 847, 657, 576, 458 and 408 F g^{-1} at scan rates of 5, 10, 20, 30, 40, 50, 75 and 100 mV s^{-1}, respectively. From the above-calculated value it is observed that the calculated specific capacitance decreases with increase in the scan rates, this is due to the faster mobility of the electrolyte ions and as a result not able to entirely participate in the electrochemical reaction with the active material at higher scan rates [40]. Figure 8 shows the GCD curves at various current densities with a potentials window between 0 and 0.4 V for $MnCo_2O_4$. From Fig. 8, it is observed that the quasi-symmetric charge/discharge curve propose that the pseudocapacitive behavior of the material and were calculated the specific capacitances using the Eq. (2). Figure 9 shows the decrease in the specific capacitance 1617, 1505, 1395, 1390, 1250, and 900 F g^{-1} with respect to the different discharge current densities 1, 2, 3, 4, 5, and 10 A g^{-1} for the $MnCo_2O_4$. From Fig. 9, it is observed that an increase in the

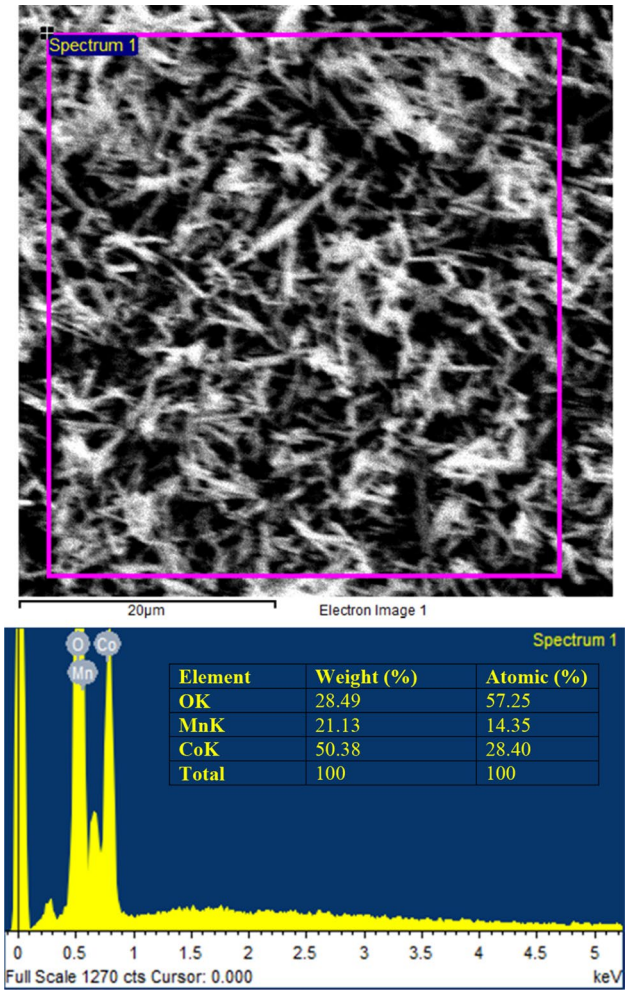

Fig. 5 EDS spectrum of the $MnCo_2O_4$ nanorods calcined at 400 °C for 3 h

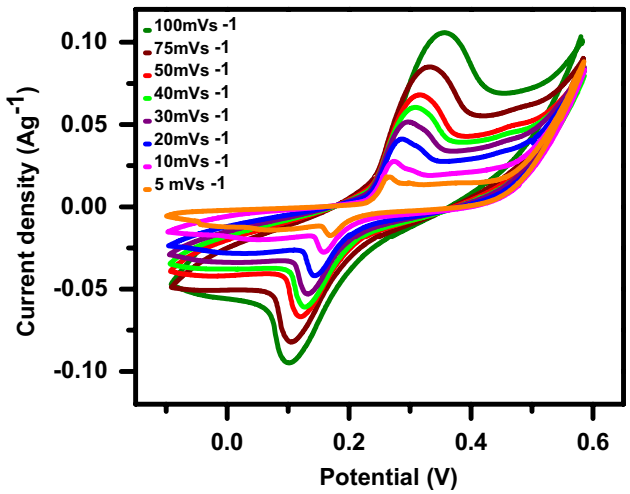

Fig. 6 CV curves of the $MnCo_2O_4$ electrode in 1 M KOH electrolyte at different scan rates

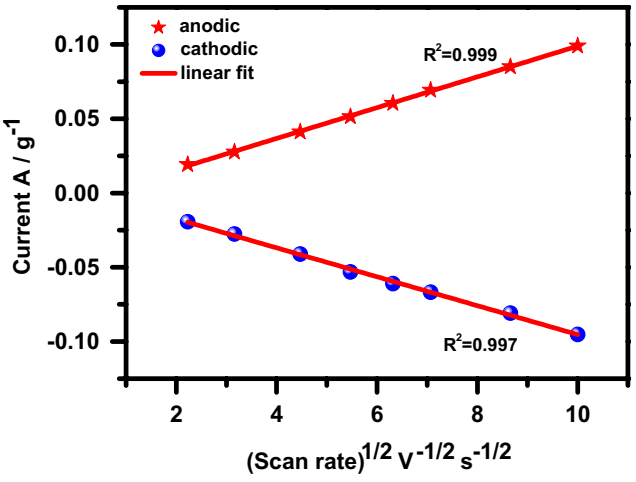

Fig. 7 Peak current versus square root of scan rate plots of $MnCo_2O_4$ nanorods

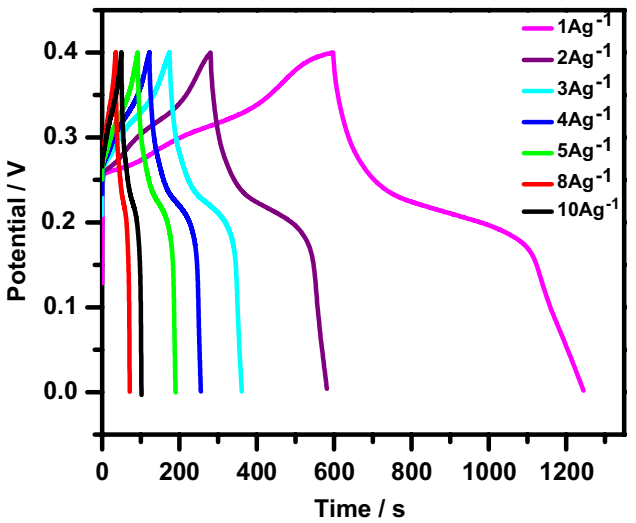

Fig. 8 GCD curves of the $MnCo_2O_4$ electrode with different discharge current densities in 1 M KOH as an electrolyte

current density results in the capacitance decrease, which may be attributed to a reduction in diffusion of OH^- ion into the active sites of electrode material [41]. The electrochemical reaction demonstrated the highest specific capacitance of 1617 F g^{-1} at a current density 1 A g^{-1}.

The GCD curves at a current density of 20, 30, 50 and 100 A g^{-1} are shown in Fig. 10. From Fig. 10 it is observed that the shape of quasi-symmetric charge/discharge curve does not change even at a high current (100 A g^{-1}) and the electrode retains the capacitance of 275 F g^{-1} (17%). The above result proves the excellent stability of the electrode materials and it is due to the morphology of bundles of $MnCo_2O_4$ nanorods bundles like structural features, such a high current structural stability is extremely essential for the

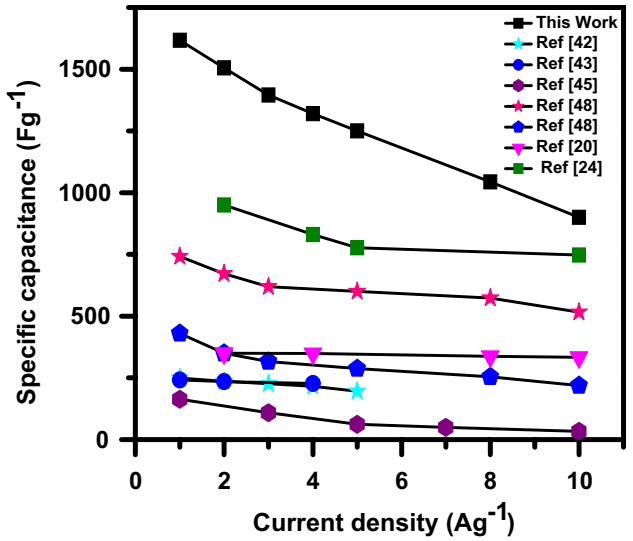

Fig. 9 Specific capacitance of the $MnCo_2O_4$ electrodes calculated from GCD analysis and compared with literature reports

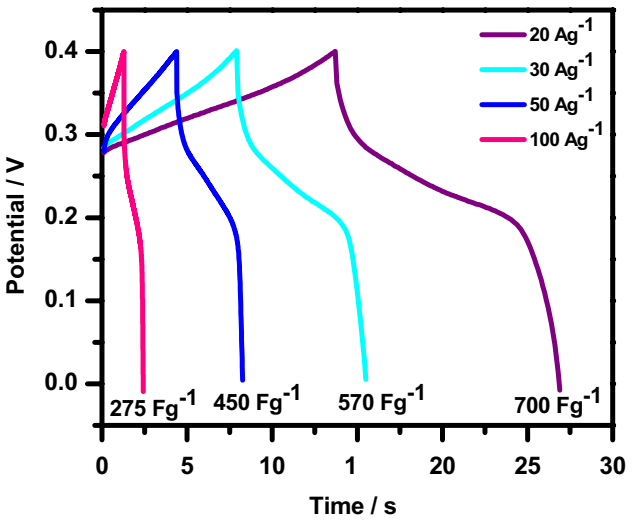

Fig. 10 GCD curves of the $MnCo_2O_4$ electrode at 20, 30, 50 and 100 A g^{-1} discharge current densities in 1 M KOH as an electrolyte

applicability of the $MnCo_2O_4$ materials for the supercapacitor. Thus, in the present work, the obtained specific capacitance of the $MnCo_2O_4$ nanorod bundles synthesized via the MH method is comparatively higher than the literature reports. The comparison of few literature reports such as Li et al., reported a high specific capacitance of 349.8 F g^{-1} for $MnCo_2O_4$ nanowire arrays on nickel foam by hydrothermal method at a current density of 1 A g^{-1} [20]. Venkatachalam et al., reported the high specific capacitance of 507.5 F g^{-1} for the $MnCo_2O_4$ nanostructured electrode at a current density of 1 A g^{-1} [22]. Table 1 represents the comparison of the specific capacitances reported in the literature with the present work.

The GCD measurement was carried out at different current densities 5, 10, 20, 30, 50 and 100 A g^{-1} for 120 cycles are shown in Fig. 11. From Fig. 11 it is observed that the $MnCo_2O_4$ nanorods bundle-like structure electrode material exhibit the high reversible capacity, high capacitance retention performance and excellent cycling stability as the cycling current was varied from low (5 A g^{-1}) to high (100 A g^{-1}) current and reversed back to a current at 5 A g^{-1}. Thus, the high rate performances and good reversible capacity retention at different current densities demonstrate the structural stability of the calcined $MnCo_2O_4$ nanorods bundles, which is capable of delivering required high energy at various load levels and confirm to be a promising electrode material for supercapacitors application [42].

The cycling performance is significant for the electrode materials in supercapacitor applications [44]. The cyclic stability test of the electrodes was carried out using GCD measurement at a current density of 10 A g^{-1} for 1000 cycles. Figure 12 shows the specific capacitance and the capacitance retentions with respect to a number of cycles and the inset fig. shows the first ten charge/discharge cycles of $MnCo_2O_4$ nanorods. From Fig. 12, it is observed that about 88% of initial capacitance was retained even after 1000 cycles at a high current density of 10 A g^{-1}, which demonstrates the good cyclic stability of the $MnCo_2O_4$ material as the electrode even at high current.

EIS of the electrodes are measured in an open circuit potential at a frequency range from 10 kHz to 1 Hz after 1st and 1000th cycles at a current density of 10 A g^{-1} is shown in Fig. 13. From Fig. 13, it is observed that the presence of a depressed semi-circle at the higher frequency region is attributed to the combination of parallel circuits of capacitance and the ionic charge transfer resistance. The presence inclined straight line at the low-frequency region represents the Warburg resistance (Zw). It is also observed that this is due to the frequency dependent ion-diffusion or transport in the electrolyte to the electrode surface [44]. From the figure, it is noted that the slight increase in the radius of the depressed semicircle at high-frequency region after the 1000th cycle compared with the 1st cycle reveals the small decrease in the interfacial charge transfer conductivity of electrodes. At low-frequency region, Warburg resistance slightly increased after 1000 cycles and the slope was not altered, which suggest the mobility of the ions in the electrolyte to the electrode surface was not relatively altered. The internal drop in the specific capacitance can be attributed to the slight decrease in the interfacial charge transfer conductivity, which causes a decrease in the retention of the initial capacitance for $MnCo_2O_4$ during the cycle performance. The overall results suggested that the MH synthesized

Table 1 Comparison of the specific capacitances of the $MnCo_2O_4$ nanorod electrodes with the literature reports for supercapacitor applications

S. no.	Material	Synthesis method	Specific capacitance (F g^{-1})	Scan rate mV s^{-1} (or) current density (A g^{-1})	Refs.
1	$MnCo_2O_4$	Hydrothermal method	349.8 F g^{-1}	1 A g^{-1}	[20]
2	$MnCo_2O_4$	Solvothermal process	346 F g^{-1}	1 A g^{-1}	[32]
3	$MnCo_2O_4$	Hydrothermal method	507.5 F g^{-1}	1 A g^{-1}	[22]
4	$MnCo_2O_4$	Electrodeposition	250 F g^{-1}	0.25 A g^{-1}	[17]
5	$MnCo_2O_4$	Solvothermal method	235.7 F g^{-1}	1 A g^{-1}	[42]
6	$MnCo_2O_{4.5}$	Hydrothermal method	118.8 F g^{-1} 151.2 F g^{-1}	1 A g^{-1} 5 mV s^{-1}	[43]
7	$MnCo_2O_{4.5}$/graphene	Hydrothermal process	255.8 F g^{-1}	5 mV s^{-1}	[44]
8	$MnCo_2O_4$	Solvothermal synthesis	539 F g^{-1}	1 A g^{-1}	[45]
9	$MnCo_2O_4$	Hydrothermal method	600 F g^{-1}	0.5 A g^{-1}	[46]
10	$MnCo_2O_4$	Hydrothermal method	480.5 F g^{-1}	1 A g^{-1}	[47]
11	$MnCo_2O_4$ C@$MnCo_2O_4$	Hydrothermal method	430 F g^{-1} 728 F g^{-1}	1 A g^{-1} 1 A g^{-1}	[48]
12	$MnCo_2O_4$ grown on nickel foam	Hydrothermal method	1535 F g^{-1}	1 A g^{-1}	[18]
13	$MnCo_2O_4$ nanorods	Microwave hydrothermal method	2394.4 F g^{-1} 1617.5 F g^{-1}	5 mV s^{-1} 1 A g^{-1}	Present Work

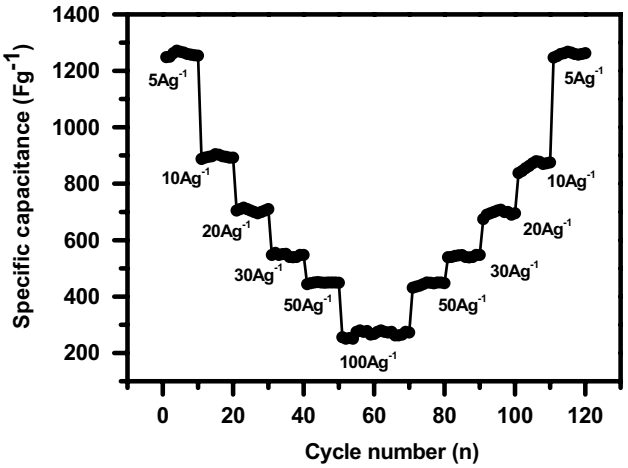

Fig. 11 Cycle stability test of the $MnCo_2O_4$ nanorods electrode at various current densities for 120 cycles

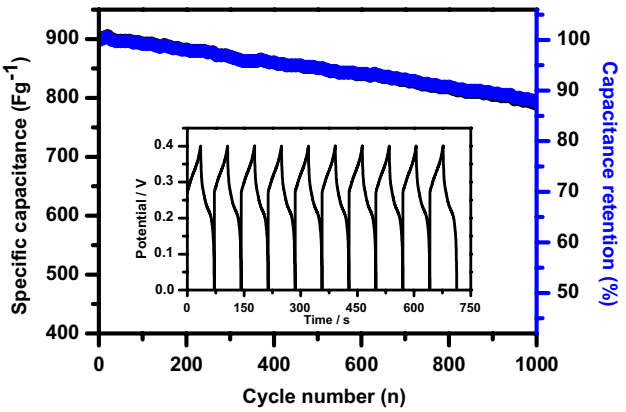

Fig. 12 Cycling performance of in the $MnCo_2O_4$ electrode at a current density of 10 A g^{-1} (inset figure shows the first ten GCD cyclic profiles)

$MnCo_2O_4$ nanorods bundles would be a promising electrode material for the supercapacitor applications.

The variations of the energy density as a function of the power density for the $MnCo_2O_4$ electrodes are shown in Fig. 14. The energy density and power density were derived from charge/discharge curves at various current densities and these can be calculated from the following equations [30].

$$E = \frac{1}{2}C_s(\Delta V)^2 \text{Wh kg}^{-1} \quad (3)$$

$$P = \frac{Q\Delta C}{2T} = \frac{E}{T} \text{ W kg}^{-1} \quad (4)$$

where P is the power density (W kg^{-1}), E is the energy density (Wh kg^{-1}), Cs is the specific capacitance based on the mass of the electroactive material (F g^{-1}), Q is the total charge delivered (C), ΔV is the potential window of discharge (V), and t is the discharge time (s). From Fig. 14, it is observed that the energy density decreases with an increase in the power density. The maximum energy density obtained for the electrodes 35.9 and 27 Wh kg^{-1} at the power density of 200 and 1000 W kg^{-1}. The obtained energy density is higher than the literature reports such as C@$MnCo_2O_4$ (25.5 Wh kg^{-1} at 856 W kg^{-1}) [48], $NiMn_2O_4$ (3.6 Wh kg^{-1} at 224.76 W kg^{-1}) [47], C@$NiMn_2O_4$ (13.23 Wh kg^{-1} at 224.76 W kg^{-1}) [49], $MnMoO_4$ (15.5 Wh kg^{-1} at 224.9 W kg^{-1}) [27], $NiMn_2O_4$ (29.64 Wh kg^{-1} at

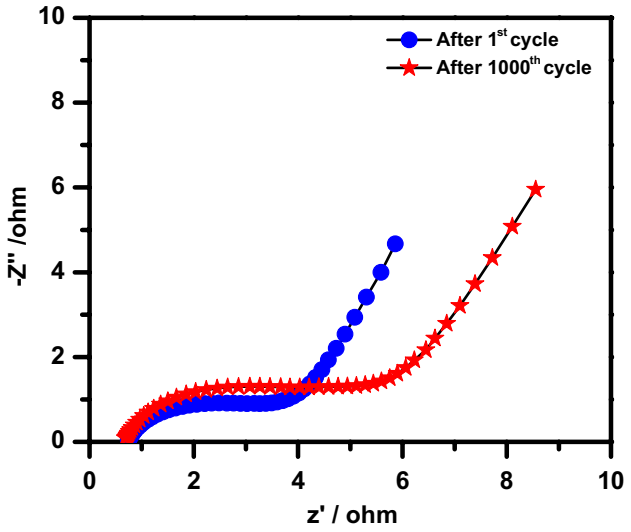

Fig. 13 Electrochemical impedance spectra of the $MnCo_2O_4$ electrode after 1st and 1000 GCD cycles at a current density of 10 A g^{-1}

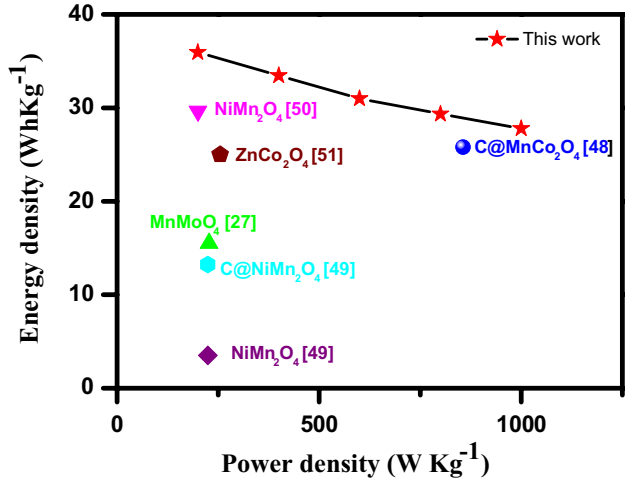

Fig. 14 Ragone plots (power density versus energy density) of the $MnCo_2O_4$ nanorods electrode with literature report

200.27 W kg^{-1}) [50], $ZnCo_2O_4$ (25 Wh kg^{-1} at 255 W kg^{-1}) [51]. The high energy density without any significant loss of the power density demonstrated that the $MnCo_2O_4$ nanorods bundle-like structure is vital to consider as an efficient supercapacitor electrode materials.

4 Conclusion

$MnCo_2O_4$ nanorods have been successfully synthesized via the MH methods. $MnCo_2O_4$ electrode exhibited an excellent specific capacitance of 1617.5 F g^{-1} at the current density of 1 A g^{-1}. The cycling stability had revealed a good reversibility, with a cycling efficiency of 88% after 1000 cycles at a high current density of 10 A g^{-1}. The high rate performances and good reversible capacity retention at different current densities demonstrated the structural stability of the calcined $MnCo_2O_4$. Thus, the facile MH approach to synthesis $MnCo_2O_4$ nanorod may be a valuable method to obtain a promising electrode with a high electrochemical performance for the supercapacitor applications.

Acknowledgements Authors are grateful to PFRC and BRNS, DAE, Govt. of India, for utilizing the instruments purchase under the various funded project.

References

1. H. Wang, Y. Yang, Y. Liang, J.T. Robinson, Y. Li, A. Jackson, Y. Cui, H. Dai, Graphene wrapped sulfur particles as a rechargeable lithium–sulfur battery cathode material with high capacity and cycling stability. Nano Lett. **11**, 2644–2647 (2011)
2. F. Shi, L. Li, X.L. Wang, C.D. Gu, J.P. Tu, Metal oxide/hydroxide-based materials for supercapacitors. RSC Adv. **4**, 41910–41921 (2014)
3. Y. Yang, T. Liu, L. Zhang, S. Zhao, W. Zeng, S. Hussain, C. Deng, H. Pan, X. Peng, Facile synthesis of nickel doped walnut-like MnO_2 nanoflowers and their application in a supercapacitor. J Mater Sci. Mater. Electron. **27**, 6202–6207 (2016)
4. R. Ramkumar, M. Minakshi, Sundaram, Electrochemical synthesis of polyaniline cross-linked $NiMoO_4$ nanofibre dendrites for energy storage devices. New J. Chem. **40**, 7456–7464 (2016)
5. B. Li, Q. Sun, R. Yang, D. Li, Z. Li, Simple preparation of graphene-decorated $NiCo_2O_4$ hollow nanospheres with enhanced performance for supercapacitor. J. Mater. Sci. Mater. Electron. **29**, 7681–7691 (2018)
6. S. Biswas, L.T. Drzal, Multilayered nano-architecture of variable sized graphene nanosheets for enhanced supercapacitor electrode performance. ACS Appl. Mater. Interfaces **2**, 2293–2300 (2010)
7. G.S. Gund, D.P. Dubal, S.S. Shinde, C.D. Lokhande, One step hydrothermal synthesis of micro-belts like β-Ni $(OH)_2$ thin films for supercapacitors. Ceram. Int. **39**, 7255–7261 (2013)
8. K. Adib, M.R. Nasrabadi, Z. Rezvani, S.M. Pourmortazavi, F. Ahmadi, H.R. Naderi, M.R. Ganjali, Facile chemical synthesis of cobalt tungstates nanoparticles as high performance supercapacitor. J Mater Sci. Mater. Electron. **27**, 4541–4550 (2016)
9. H. Wang, Y. Yang, Y. Liang, G. Zheng, Y. Li, Y. Cui, H. Dai, Rechargeable Li–O_2 batteries with a covalently coupled $MnCo_2O_4$–graphene hybrid as an oxygen cathode catalyst. Energy Environ. Sci. **5**, 7931–7935 (2012)
10. Y. Liang, H. Wang, J. Zhou, Y. Li, J. Wang, T. Regier, H. Dai, Covalent hybrid of spinel manganese-cobalt oxide and graphene as advanced oxygen reduction electrocatalysts. J. Am. Chem. Soc. **134**, 3517–3523 (2012)
11. J. Li, S. Xiong, X. Li, Y. Qian, Spinel $Mn_{1.5}Co_{1.5}O_4$ core–shell microspheres as Li-ion battery anode materials with a long cycle life and high capacity. J. Mater. Chem. **22**, 23254–23259 (2012)
12. H. Chen, J. Jiang, L. Zhang, T. Qi, D. Xia, H. Wan, Facilely synthesized porous $NiCo_2O_4$ flowerlike nanostructure for high-rate supercapacitors. J. Power Sources **248**, 28–36 (2014)
13. Q. Zhou, J. Xing, Y. Gao, X. Lv, Y. He, Z. Guo, Y. Li, Ordered assembly of $NiCo_2O_4$ multiple hierarchical structures for high-performance pseudocapacitors. Appl. Mater. Interfaces **6**, 11394–11402 (2014)

14. A. Pendashteh, S.E. Moosavifard, M.S. Rahmanifar, Y. Wang, M.F. El-Kady, R.B. Kaner, M.F. Mousavi, Highly ordered mesoporous $CuCo_2O_4$ nanowires, a promising solution for high-performance supercapacitors. Chem. Mater. **27**, 3919–3926 (2015)
15. S.G. Krishnan, M.V. Reddy, M. Harilal, B. Vidyadharan, I.I. Misnon, M.H.A. Rahim, J. Ismail, R. Jose, Characterization of $MgCo_2O_4$ as an electrode for high performance supercapacitors. Electrochim. Acta **161**, 312–321 (2015)
16. Y. Xu, X. Wang, C. An, Y. Wang, L. Jiao, H. Yuan, Facile synthesis route of porous $MnCo_2O_4$ and $CoMn_2O_4$ nanowires and their excellent electrochemical properties in supercapacitors. J. Mater. Chem. A **2**, 16480–16488 (2014)
17. S. Sahoo, K.K. Naik, C.S. Rout, Electrodeposition of spinel $MnCo_2O_4$ nanosheets for supercapacitor applications. Nanotechnology **26**, 455401 (2015)
18. K.N. Hui, K.S. Hui, Z. Tang, V.V. Jadhav, Q.X. Xia, Hierarchical chestnut-like $MnCo_2O_4$ nanoneedles grown on nickel foam as binder-free electrode for high energy density asymmetric supercapacitors. J. Power Sources **330**, 195–203 (2016)
19. R. Krishnapriya, S. Praneetha, A. Vadivel, Murugan, Energy-efficient, microwave-assisted hydro/solvothermal synthesis of hierarchical flowers and rice grain-like ZnO nanocrystals as photoanodes for high performance dye-sensitized solar cells. CrystEngComm **17**, 8353–8367 (2015)
20. L. Li, Y.Q. Zhang, X.Y. Liu, S.J. Shi, X.Y. Zhao, H. Zhang, X. Ge, G.F. Cai, C.D. Gu, X.L. Wang, J.P. Tu, One-dimension $MnCo_2O_4$ nanowire arrays for electrochemical energy storage. Electrochim. Acta **116**, 467–474 (2014)
21. B. Kong, C. Lu, M.C. Liu, Y.C. Luo, L. Kang, X. Li, F.C. Walsh, The specific capacitance of sol–gel synthesised spinel $MnCo_2O_4$ in an alkaline electrolyte. Electrochim. Acta **115**, 22–27 (2014)
22. V. Venkatachalam, A. Alsalme, A. Alghamdi, R. Jayavel, High performance electrochemical capacitor based on $MnCo_2O_4$ nanostructured electrode. J. Electroanal. Chem. **756**, 94–100 (2015)
23. S.G. Krishnan, M.H.A. Rahim, R. Jose, Synthesis and characterization of $MnCo_2O_4$ cuboidal microcrystals as a high performance psuedocapacitor electrode. J. Alloys Compd. **656**, 707–71365 (2016)
24. G.M. Thorat, H.S. Jadhav, J. Gil Seo, Bi-functionality of mesostructured $MnCo_2O_4$ microspheres for supercapacitor and methanol electro-oxidation. Ceram. Int. **43**, 2670–2679 (2017)
25. Y. Dong, Y. Wang, Y. Xu, C. Chen, Y. Wang, L. Jiao, H. Yuan, Facile synthesis of hierarchical nanocage $MnCo_2O_4$ for high performance supercapacitor. Electrochim. Acta **225**, 39–46 (2017)
26. M.C. Liu, L.B. Kong, C. Lu, X.J. Ma, X.M. Li, Y.C. Luob, L. Kang, Design and synthesis of $CoMoO_4$–$NiMoO_4.H_2O$ bundles with improved electrochemical properties for supercapacitors. J. Mater. Chem. A **1**, 1380–1387 (2013)
27. I. Bilecka, M. Niederberger, Microwave chemistry for inorganic nanomaterials synthesis. Nanoscale **2**, 1358–1374 (2010)
28. M. Baghbanzadeh, S.D. Škapin, Z.C. Orel, C.O. Kappe, A critical assessment of the specific role of microwave irradiation in the synthesis of ZnO micro- and nanostructured materials. Chem. Eur. J. **18**, 5724–5731 (2012)
29. Y. Yang, Y. Liang, J. Hu, J. Zou, Q. Tang, Z. Wan, Y. Lu, Rapid microwave-assisted hydrothermal synthesis of hierarchical micro/nanostructured TiO_2 with tunable nanomorphologies. J Mater Sci. Mater. Electron. **27**, 11606–11612 (2016)
30. S. Jayasubramaniyan, S. Balasundari, P.A. Rayjada, N. Satyanarayana, P. Muralidharan, Microwave hydrothermal synthesis of α-$MnMoO_4$ nanorods for high electrochemical performance supercapacitors. RSC Adv. **8**, 22559–22568 (2018)
31. S. Ma, L. Sun, L. Cong, X. Gao, C. Yao, X. Guo, L. Tai, P. Mei, Y. Zeng, H. Xie, R. Wang, Multiporous $MnCo_2O_4$ microspheres as efficient bifunctional catalyst for non aqueous Li–O_2 batteries. J. Phys. Chem. C **117**, 25890–25897 (2013)
32. N. Padmanatha, S. Selladurai, Mesoporous $MnCo_2O_4$ spinel oxide nanostructure synthesized by solvothermal technique for supercapacitor. Ionics **20**, 479–487 (2014)
33. J. Pal, P. Chauhan, Study of physical properties of cobalt oxide (Co_3O_4) nanocrystals. Mater. Charact. **61**, 575–579 (2010)
34. R. Tholkappiyan, A.N. Naveen, S. Sumithra, K. Vishista, Investigation on spinel $MnCo_2O_4$ electrode material prepared via controlled and uncontrolled synthesis route for supercapacitor application. J. Mater. Sci. **50**, 5833–5843 (2015)
35. D. Cai, B. Liu, D. Wang, Y. Liu, L. Wang, H. Li, Y. Wang, C. Wang, Q. Li, T. Wang, Enhanced performance of supercapacitors with ultrathin mesoporous $NiMoO_4$ nanosheets. Electrochim. Acta **125**, 294–301 (2014)
36. I. Shakir, M. Shahid, H.W. Yang, D.J. Kang, Structural and electrochemical characterization of alpha-MoO_3 nanorod-based electrochemical energy storage devices. Electrochim. Acta **56**, 376–380 (2010)
37. X. Cao, J. Wei, Y. Luo, Z. Zhou, Y. Zhang, Spherical nickel hydroxide composite electrode. Int. J. Hydrog. Energy **25**, 643–647 (2000)
38. P. Vinothbabu, P. Elumalai, Tunable supercapacitor performance of potentiodynamically deposited urea-doped cobalt hydroxide. RSC Adv. **4**, 31219–31225 (2014)
39. K. Liu, Z. Hu, R. Xue, J. Zhang, J. Zhu, Electropolymerization of high stable poly(3,4-ethylenedioxythiophene) in ionic liquids and its potential applications in electrochemical capacitor. J. Power Sources **179**, 858–862 (2008)
40. S. Saranya, R.K. Selvan, N. Priyadharsini, Synthesis and characterization of polyaniline/$MnWO_4$ nanocomposites as electrodes for pseudocapacitors. Appl. Surf. Sci. **258**, 4881–4887 (2012)
41. P. Justin, G.R. Rao, CoS spheres for high-rate electrochemical capacitive energy storage application. Int. J. Hydrog. Energy **35**, 9709–9715 (2010)
42. H. Chen, A. Liu, J. Mu, C. Wu, X. Zhang, Template-free synthesis of novel flower-like $MnCo_2O_4$ hollow microspheres for application in supercapacitors. Ceram. Int. **42**, 2416–2424 (2016)
43. W. Li, K. Xu, G. Song, X. Zhou, R. Zou, J. Yang, Z. Chena, J. Hu, Facile synthesis of porous $MnCo_2O_{4.5}$ hierarchical architectures for high-rate supercapacitors. CrystEngComm **16**, 2335–2339 (2014)
44. Y. Li, X. Peng, J. Xiang, J. Yang, Synthesis of $MnCo_2O_{4.5}$/graphene composite as electrode material for supercapacitors. Int. J. Electrochem. Sci. **12**, 10763–10772 (2017)
45. H. Che, Y. Wang, Y. Mao, Novel flower-like $MnCo_2O_4$ microstructure self-assembled by ultrathin nanoflakes on the microspheres for high-performance supercapacitors. J. Alloys Compd. **680**, 586–594 (2016)
46. S.G. Krishnan, M. Hasbi, A. Rahim, R. Jose, Synthesis and characterization of $MnCo_2O_4$ cuboidal microcrystals as a high performance psuedocapacitor electrode. J. Alloys Compd. **656**, 707–713 (2016)
47. M. Li, W. Yang, J. Li, M. Feng, W. Li, H. Li, Y. Yu, Porous layered stacked $MnCo_2O_4$ cubes with enhanced electrochemical capacitive performance. Nanoscale **10**, 2218–2225 (2018)
48. L. Li, F. He, S. Gai, S. Zhang, P. Gao, M. Zhang, Y. Chen, P. Yang, Hollow structured and flower-like C@$MnCo_2O_4$ composite for high electrochemical performance in a supercapacitor. CrystEngComm **16**, 9873–9881 (2014)
49. M.R. Kim, R.M. NaiduKalla, S. Kim, M.-R. Kim, I. Kim, $NiMn_2O_4$ nanosheet-decorated hierarchically porous

polyaromatic carbon spheres for high-performance supercapacitors. ChemElectroChem **4**, 1–9 (2017)
50. H. Wei, J. Wang, L. Yu, Y. Zhang, D. Hou, T. Li, Facile synthesis of $NiMn_2O_4$ nanosheet arrays grown on nickel foam as novel electrode materials for high-performance supercapacitors. Ceram. Int. **42**, 14963–14969 (2016)
51. G. Zhou, J. Zhu, Y. Chen, L. Mei, X. Duan, G. Zhang, L. Chen, T. Wang, B. Lu, Simple method for the preparation of highly porous $ZnCo_2O_4$ nanotubes with enhanced electrochemical property for supercapacitor. Electrochim. Acta **123**, 450–455 (2014)